Geophysical Journal International

Geophys. J. Int. (2015) **202,** 1522–1534 doi: 10.1093/gji/ggv240
GJI Marine geosciences and applied geophysics

Improved gravity anomaly fields from retracked multimission satellite radar altimetry observations over the Persian Gulf and the Caspian Sea

M. Khaki,[1,2,3] E. Forootan,[1,4] M.A. Sharifi,[2,3] J. Awange[1] and M. Kuhn[1]

[1] *Western Australian Centre for Geodesy and The Institute for Geoscience Research, Curtin University, Perth, Australia. E-mail: forootan@geod.uni-bonn.de*
[2] *Faculty of Surveying and Geospatial Engineering, College of Engineering, University of Tehran, Iran*
[3] *Research Institute of Geoinformation Technology (RIGT), College of Engineering, University of Tehran, Iran*
[4] *Institute of Geodesy and Geoinformation, Bonn University, Nussallee 17, D-53115, Bonn, Germany*

Accepted 2015 June 3. Received 2015 June 3; in original form 2014 December 26

SUMMARY

Satellite radar altimetry observations are used to derive short wavelength gravity anomaly fields over the Persian Gulf and the Caspian Sea, where *in situ* and ship-borne gravity measurements have limited spatial coverage. In this study the retracking algorithm 'Extrema Retracking' (ExtR) was employed to improve sea surface height (SSH) measurements that are highly biased in the study regions due to land contaminations in the footprints of the satellite altimetry observations. ExtR was applied to the waveforms sampled by the five satellite radar altimetry missions: TOPEX/POSEIDON, JASON-1, JASON-2, GFO and ERS-1. Along-track slopes have been estimated from the improved SSH measurements and used in an iterative process to estimate deflections of the vertical, and subsequently, the desired gravity anomalies. The main steps of the gravity anomaly computations involve estimating improved SSH using the ExtR technique, computing deflections of the vertical from interpolated SSHs on a regular grid using a biharmonic spline interpolation and finally estimating gridded gravity anomalies. A remove–compute–restore algorithm, based on the fast Fourier transform, has been applied to convert deflections of the vertical into gravity anomalies. Finally, spline interpolation has been used to estimate regular gravity anomaly grids over the two study regions. Results were evaluated by comparing the estimated altimetry-derived gravity anomalies (with and without implementing the ExtR algorithm) with ship-borne free air gravity anomaly observations, and free air gravity anomalies from the Earth Gravitational Model 2008 (EGM2008). The comparison indicates a range of 3–5 mGal in the residuals, which were computed by taking the differences between the retracked altimetry-derived gravity anomaly and the ship-borne data. The comparison of retracked data with ship-borne data indicates a range in the root-mean-square-error (RMSE) between approximately 1.8 and 4.4 mGal and a bias between 0.4062 and 2.1413 mGal over different areas. Also a maximum RMSE of 4.4069 mGal, with a mean value of 0.7615 mGal was obtained in the residuals. An average improvement of 5.2746 mGal in the RMSE of the altimetry-derived gravity anomalies corresponding to 89.9 per cent was obtained after applying the ExtR post-processing.

Key words: Satellite geodesy; Sea level change; Gravity anomalies and Earth structure.

1 INTRODUCTION

Satellite radar altimetry has wide applications in oceanography, the estimation of variations in sea level and large inland water bodies and climate change (e.g. Fu *et al.* 1994; Shum *et al.* 1995), as well as in geodynamics and physical geodesy, where it provides dense and precise sea surface height (SSH) measurements all over the world (Hwang & Hsu 2003). Satellite radar altimetry data has been used to study ocean tectonics in Lawver *et al.* (1992), Cande *et al.* (2000), Fernandes *et al.* (2001) and Sandwell *et al.* (2014), as well as to estimate the marine gravity field in Haxby *et al.* (1983), Cazenave & Royer (2001) and Hwang *et al.* (1998). Altimeter observations of SSH also offer a fundamentally different way to measure more localized gravity anomalies than those provided by space satellite gravity missions, such as CHAMP[1], GRACE[2] or GOCE[3]

[1] Challenging Minisatellite Payload (CHAMP).
[2] The Gravity Recovery And Climate Experiment (GRACE).
[3] Gravity field and steady-state Ocean Circulation Explorer (GOCE).

(Andersen *et al.* 2008; Sandwell & Smith 2009), while these space satellite gravity missions provide rather precise gravity field observations at longer wavelength (e.g. a resolution of ∼100 km or longer for GRACE static field) based on a long-term average (e.g. ITG2010S; Mayer-Gürr 2006), they cannot provide more localized information. Therefore, satellite radar altimetry can be used to improve the knowledge about gravity anomalies primarily at wavelengths of ∼100 km and shorter by measuring sea surface topography. In fact, the higher resolution of the gravity field inferred from satellite altimetry is due to the nature of measurements that reflect gravity anomalies close to the earth's crust, which is primarily responsible for gravity field variations of the wavelength of 5–100 km (Andersen *et al.* 2008, 2010; Sandwell *et al.* 2014).

Numerous studies exist that demonstrated the application of satellite radar altimetry at both global (e.g. Sandwell & Smith 1997, 2009; Hwang *et al.* 1998) and local scales (e.g. Noreus *et al.* 1997; Andersen & Kundsen 2000). In this study, altimetry measurements are applied to investigate short wavelength gravity anomalies over the Persian Gulf and the Caspian Sea. The main aim of our study is to improve the static gravity field over both study areas using improved SSH measurements from retracked satellite altimetry waveforms. The motivation for selecting these study areas originates from the fact that both regions are characterized by complex geophysical processes. The Persian Gulf, with a surface area of ∼251 000 km^2, is an east–west stretch of shallow water body (average depth of ∼50 m), located where the Arabian Plate (from south) meets the Eurasian Plate (in north). As a result, temporally gravity changes can be detected over the southern part of Iran and the Persian Gulf (Perotti *et al.* 2011; Forootan *et al.* 2014). More geophysical phenomena, such as a sea level rise caused by post-glacial rebound, have also been reported, e.g. in Lambeck *et al.* (2002). A large geoid height change of ∼20 m in north–south direction is present over the Caspian Sea, the world's largest lake (∼371 000 km^2), where two tectonic plates meet at the south Caspian Basin (Jackson *et al.* 2002). To the best of our knowledge, very few attempts have been undertaken to monitor gravity anomalies over these regions using satellite altimetry observations (e.g. Sandwell & Smith 1997; Ozyavas *et al.* 2010; Safari *et al.* 2014). This contribution adds to the previous literature by providing high-resolution gravity field maps over the Persian Gulf and the Caspian Sea using improved altimetry-derived SSH based on the retracking algorithm ExtR (Khaki *et al.* 2014).

The altimetry data used in this study consists of waveform observations of the Topex/Poseidon, Jason-1, Jason-2, Geosat Follow-On (GFO) and ERS-1 missions. Our motivation to select these altimetry missions is due to their high density coverage over both the Persian Gulf and the Caspian Sea. Using various missions with different satellite footprints is necessary for precise estimation of gravity anomalies (Sandwell & Smith 1997). To estimate gravity anomaly from altimetry measurements, various important steps must be undertaken (Sandwell & Smith 2009) of which measuring SSH accurately is the most important consideration.

Radar altimeters measure heights of the surface of water bodies, which in first approximation, is related to the gravitational potential (e.g. Garcia *et al.* 2014). Knowing that gravity anomalies are the vertical derivative of the Earth's potential field, a precise estimation of sea surface slope is essential. Sandwell & Smith (1997) state that 1 mGal of change in gravity anomaly approximately corresponds to 1 μrad (micro-radian) of ocean surface slope.

In fact, many factors affect the absolute height accuracy of altimetry-derived SSH, and subsequently sea surface slopes. These include, for example, errors in orbital positions, atmospheric errors, that is, the wet tropospheric propagation errors, as well as other corrections, such as imperfect reduction of tidal effects (see e.g. Kouraev *et al.* 2011; Sharifi *et al.* 2013; Fernandes *et al.* 2014). In addition, a crucial component in the error budget for altimetry-derived gravity estimations originates from the imperfect estimation of the 'range' (the distance between satellite and water surface) using radar measurements (Garcia *et al.* 2014). This issue is even more critical over regions, such as inland water bodies and coastlines, where radar altimetry-derived range measurements may be affected by large errors due to land contamination in the radar signal footprint (Birkett *et al.* 2002; Berry *et al.* 2005). This issue is also critical for both study areas considered in this paper.

In order to use altimetry observations over inland water bodies and coastal areas, it is necessary to apply a post-processing algorithm (based on 'waveform retracking') to improve the accuracy of range (or SSH) estimations (Brown 1977). The 'retracking' process here refers to the re-analysis of the waveforms, a time-series of returned power in the satellite antenna, in order to improve altimetry parameters, such as range, significant wave height and wind speed (Davis 1995; Gomez-Enri *et al.* 2009). There are several studies that address the waveform retracking over inland water bodies, for example, Lee *et al.* (2008), Zhang *et al.* (2009), Troitskaya *et al.* (2012) and Uebbing *et al.* (2015). Andersen *et al.* (2010) used double retracking technique to improve the global marine gravity field. In general, no particular retracking algorithm exists that always represents optimum SSH estimations over all water bodies with different characteristics. Therefore, retracking algorithms have to be specifically designed for each particular region/application.

In this study, possible improvements in estimation of altimetry-derived gravity field due to the application of waveform retracking are assessed. Particularly, in order to retrack satellite radar altimetry data, and consequently improve SSH estimations, over the Persian Gulf and the Caspian Sea, an in-house developed algorithm, known as the Extrema Retracking (ExtR) technique proposed by Khaki *et al.* (2014) was used. The estimated altimetry-derived gravity anomalies (with or without implementing ExtR algorithm) are evaluated using ship-borne free air gravity anomaly observations, as well as free air gravity anomalies from the Earth Gravitational Model 2008 (EGM2008). Our motivation to select ExtR is due to its processing speed and its promising results over the Caspian Sea, when compared to the Off Center of Gravity (OCOG, Wingham *et al.* 1986), the NASA β-Parameter Retracking (Martin *et al.* 1983) and Threshold Retracking (Davis 1997). Khaki *et al.* (2014) indicated that estimation of geoid height profiles using the ExtR algorithm yielded improved root-mean-square-errors (RMSE) with respect to the geoid close to the coastal area of the Caspian Sea.

Various techniques exist to estimate gravity anomaly grids from altimetry-derived SSH estimates, where most are based on a remove–compute–restore procedure together with the fast Fourier transform (FFT) applied to either geoid heights or deflections of the vertical. For example, Hwang *et al.* (1998) used an inverse Vening Meinesz formulation to compute gravity anomaly in 12 different case studies including inland water bodies. The least-squares collocation technique was applied in Hwang & Hsu (2008) to estimate gravity anomalies over the China Sea and Taiwan Strait. A combination of terrestrial gravity data and satellite altimetry gravity anomalies were implemented in Kingdon *et al.* (2007) over the Great Lakes (see also Marchenko *et al.* 2003; Sandwell & Smith 2009).

In this study, the method proposed in Sandwell & Smith (2009) was used to recover gravity anomalies from ExtR-improved altimetry data over the Persian Gulf and the Caspian Sea. The applied method is based on the formulation of a boundary value problem

of the Laplace equation, which allows the extraction of gravity anomalies from deflections of the vertical using the FFT technique. Even though each of the other methods proposed in the literature has some unique advantages, the following reasons informed the choice of Sandwell & Smith's (2009) algorithm, that is, (i) many error sources that affect the accuracy of altimetry-derived absolute surface heights represent negligible influences on sea surface slope, which will be used here to estimate gravity anomalies, (ii) the algorithm is faster than other methods especially compared to that of least-square collocation and (iii) by applying this method, crossover adjustment can be avoided, which effectively allows the use of observations from different satellite altimetry missions. These factors made the implemented algorithm quite efficient in estimating gravity anomalies over localized areas, such as inland water bodies.

The remainder of this contribution is organized as follows: in Section 2, the data used in this study is explained. In Section 3, the data pre-processing, including the ExtR method, is discussed. The methodology of gravity anomaly extraction from satellite radar altimetry profiles is provided in Section 4. In Section 5, the results of deflections of the vertical and gravity anomalies over the Persian Gulf and the Caspian Sea are presented and discussed and finally in Section 6, the study is concluded.

2 DATA

2.1 Satellite radar altimetry data

The fundamental measurement type of satellite altimetry is the range between the satellite and the earth's surface, which is obtained by the traveltime of a short radar pulse. Satellite ranges should be corrected for the atmospheric influences resulting from the ionospheric and tropospheric impacts (Zhang *et al.* 2009). The reflectivity property of the sea surface also needs to be considered to correct ranges due to their influence on the shape of waveforms (Benada 1997). Since extracting short-wavelength gravity anomalies was the main goal of this study, the electromagnetic bias corrections were not considered in order to avoid introducing more noise to the altimetry-derived range products (Gille 1994). Once the corrected ranges have been computed, they were used to derive SSHs by subtracting them from precise satellite altitudes (Benada 1997).

High-density (in spatial resolution) altimetry measurements belonging to 360 cycles of T/P covering the period of 1992–2002, 260 cycles of Jason-1 covering the period of 2002–2009 and 120 cycles of Jason-2 covering the period from 2008 to 2012 were used. The temporal resolution of these observations is ∼9.915 d and their ground cross-track resolution is ∼280 km over the Persian Gulf and ∼245 km over the Caspian Sea (Benada 1997). In addition, 10 cycles of the 18-month ERS-1 mission (ESA; European Space Agency) from 1995 to 1996 with 35-d repeat orbit were used. The spatial resolution of ERS-1 satellite tracks is almost four times denser than the other satellite altimeter missions. 160 cycles of the GFO mission (U.S. Navy) covering the period of 1998–2008 with 17-d repeat orbit were also used.

Post-processing of all altimetry data sources was done in order to improve the quality of range measurements. This included using more accurate tidal and atmospheric corrections from the coastal *in situ* observations (mentioned in Section 1). Range corrections that are required to be applied to the measurements of all five satellite missions (T/P, Jason, ERS-1 and GFO) were applied following the description in Lee *et al.* (2008). These included corrections due to the atmospheric propagation, as well as geophysical surface variations (Lee *et al.* 2008). To reduce the mismatch of high frequency variations between observations of the satellite altimetry missions and *in situ* measurements, tidal frequencies were removed based on long-term high-resolution *in situ* measurements. A moving average filter with different size of window on different satellite (e.g. 10 tracking gates for the 'T/P satellite') was also applied to all surface height measurements. This is done to retain a spectral structure and to remove the short-term fluctuations while the longer term variability was left for marine gravity anomaly computation. The ground tracks of the five satellites are shown in Fig. 1, where those of (a) belong to the Persian Gulf and (b) represent the ground tracks over the Caspian Sea. In addition, Tables 1 and 2 provide details of the satellite radar altimetry data used in each study region.

2.2 Ship-borne data and gravity anomaly grids

To assess the performance of altimetry-derived gravity anomalies over the Persian Gulf, comparison was done with ship-borne derived free air gravity anomalies provided by the Iranian National Cartographic Center (NCC[4]). This data set provides a direct measurement of marine gravity anomalies which also includes short wavelength gravity variations (see the tracks of ship-borne profiles in Fig. 2). Due to the lack of ship-borne data, the gravity results belonging to the Caspian Sea were compared to the gravity anomaly grids derived from EGM2008 (Kingdon *et al.* 2007), from the International Centre for Global Earth Models (ICGEM[5]). This model includes dense gravity information derived from the combination of altimetry, satellite gravimetry and *in situ* gravity observations (GFZ; German Research Center for Geosciences, 2009). The grid over the Caspian Sea includes 3 523 801 gridpoints. This comparison was, however, only performed to assess possible biases in our gravity estimation, and cannot be used as an independent quality assessment against ground-based measurements (see e.g. Kingdon *et al.* 2007), and this is due to the fact that EGM2008 is mostly based on satellite data with rather low resolution.

3 SATELLITE ALTIMETRY RETRACKING

In order to further improve the range measurements, the ExtR post-processing technique (Khaki *et al.* 2014) was applied to the altimetry-derived waveforms. This is essential since over the Caspian Sea, complex waveform patterns are usually observed along the coastlines (specifically where water and land meets), and the northern part of the Caspian Sea that is frozen during the cold seasons (Kouraev *et al.* 2011; Khaki *et al.* 2014). Over the Persian Gulf, complex waveforms can also be found over a wide range close to the coast due to the relatively shallow water of the Gulf. It is important to mention that the retracking procedure has been applied to the data of all satellite radar altimeter missions except for the GFO mission, for which waveform data were not available.

The ExtR procedure, used in this study to retrack altimetry waveforms, is based on three main steps. First, it applies a moving average filter to reduce the random noise of the waveforms. Secondly, extremum points of the filtered waveforms are identified, and thirdly the main leading edge is found among all detected extremum points. Once the position of the leading edge in the waveforms has been defined, the offset between this position and its on-board value

[4] http://www.ncc.org.ir/

[5] http://icgem.gfz-potsdam.de/ICGEM

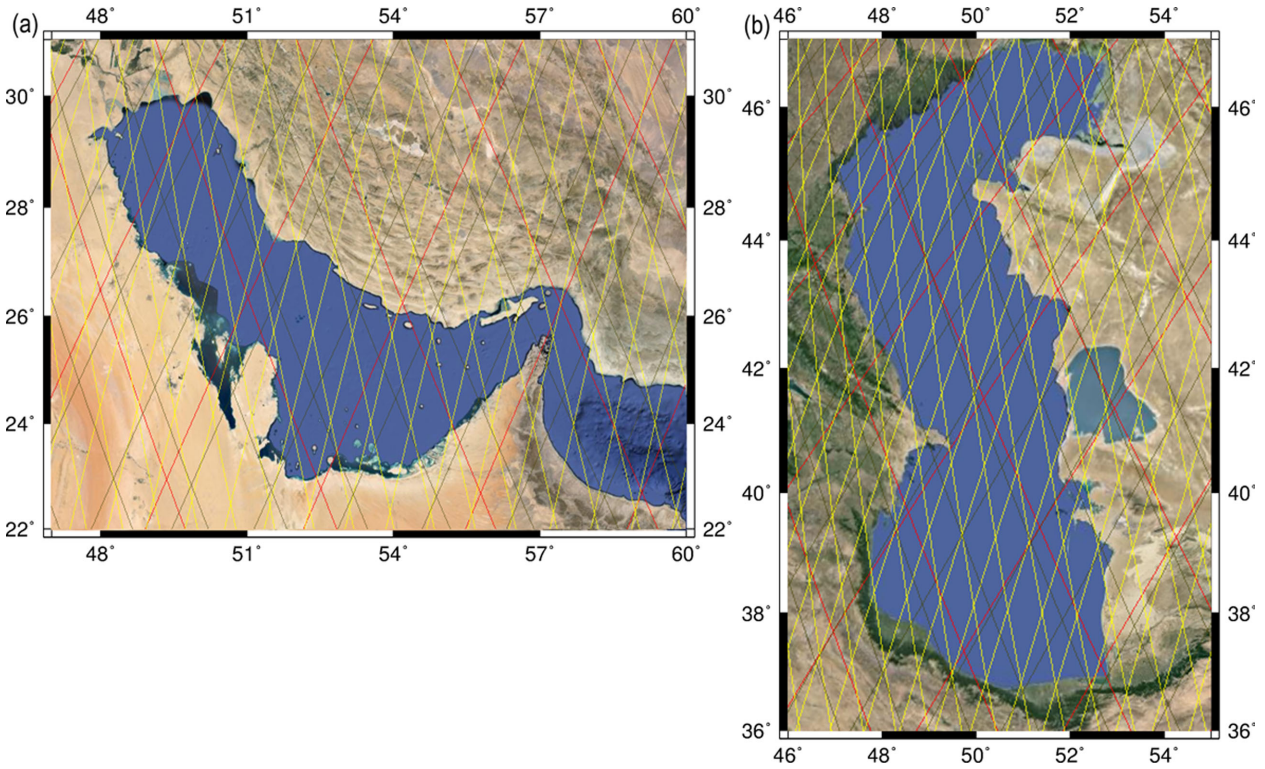

Figure 1. Ground track coverage of different satellite altimetry missions: T/P, Jason-1, Jason-2 (red), GFO (brown) and ERS-1 (yellow) over (a) the Persian Gulf and (b) the Caspian Sea. (The maps pf water bodies are generated by Google Earth, 2014.)

Table 1. Altimeter data used over the Persian Gulf.

Satellite	Number of cycles	Pass numbers
T/P	360 (1992–2002)	5, 16, 81, 92, 107, 118, 157, 183, 194, 233
Jason-1	260 (2002–2009)	5, 16, 81, 92, 107, 118, 157, 183, 194, 233
Jason-2	120 (2008–2012)	5, 16, 81, 92, 107, 118, 157, 183, 194, 233
GFO	160 (1998–2008)	12, 53, 70, 98, 111, 156, 184, 197, 242, 270, 283, 328, 369, 414, 455
ERS-1	10 (1995–1996)	12, 25, 40, 111, 126, 139, 197, 212, 225, 298, 311, 326, 384, 397, 412, 470, 483, 498, 556, 569, 584, 655, 670, 683, 756, 769, 842, 855, 870, 928, 941, 956

Table 2. Altimeter data used over the Caspian Sea.

Satellite	Number of cycles	Pass numbers
T/P	360 (1992–2002)	16, 31, 57, 92, 133, 168, 209, 244
Jason-1	260 (2002–2009)	16, 31, 57, 92, 133, 168, 209, 244
Jason-2	120 (2008–2012)	16, 31, 57, 92, 133, 168, 209, 244
GFO	160 (1998–2008)	42, 53, 70, 128, 139, 214, 255, 300, 311, 386, 397, 444, 455, 472, 483
ERS-1	10 (1995–1996)	12, 25, 98, 139, 184, 225, 270, 311, 356, 384, 397, 470, 483, 556, 597, 642, 683, 728, 769, 814, 842, 855, 900, 928, 941

is estimated and considered as the required range correction. A schematic of the ExtR algorithm is shown in Fig. 3, while its details are reported in Khaki *et al.* (2014).

To better understand the efficiency of the ExtR algorithm, a summary of statistics corresponding to the SSH errors over the Persian Gulf and the Caspian Sea is presented in Table 3. The SSH values are derived from observations of the Topex/Poseidon (T/P) mission before and after implementing the ExtR post-processing procedure. In this table, the results of retracking are compared with those of *in situ* measurements over the Persian Gulf and the Caspian Sea. Please note that all the outcomes of retracking procedure are compared with *in situ* measurements before the gravity anomaly computation process as are stated, for example, in Table 3. Over the Persian Gulf, this was applied by incorporating three tide gauges including Bandar Abbas (27.1352°E, 56.0598°N), Bushehr (28.9576°E, 50.8371°N) and Kangan (27.8353°E, 52.0594°N) located at the northern coast of the gulf. Three tide gauges, located at the southern coast of the Caspian Sea were also included to assess the computations. They include the Anzali, Noshahr and Neka ports (49.4655°E, 37.4723°N; 51.5022°E, 36.6528°N and 53.2700°E, 36.8447°N).

Considering the values in Table 3, it can be seen that the uncertainty of range estimations before and after retracking were found

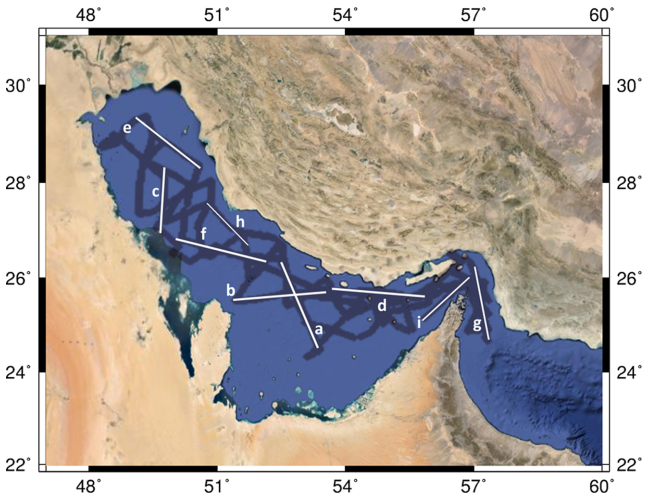

Figure 2. Ship tracks over the Persian Gulf (black lines). Sample tracks (tracks a–i) are chosen for statistical comparison of the ship-borne gravity measurements with those derived from altimetry measurements that are reported in Table 5.

to be of considerable magnitude. The results show that, for instance, after using ExtR, the RMSE over the Caspian Sea was decreased from 0.6933 to 0.4686 m when compared to tide gauge observations (29.71 per cent improvement). More quantitative details of the results over the Caspian Sea are reported in Khaki *et al.* (2014). A significant improvement of 12.98 per cent of the RMSE value was found over the Persian Gulf.

To illustrate the improvement after applying the ExtR technique, Fig. 4 presents the waveforms that are observed by Jason-2 over the Persian Gulf. The waveforms were selected from pass 16 of cycle 26, that covers a complex region which is one of the shallowest regions of the Persian Gulf and also partly covering the coastal area (see the top left graph in Fig. 4). In Fig. 4, the green and blue ellipses refer to shallower parts of the Gulf, whose complex waveforms are represented by the same coloured ellipses. Two sample waveforms were chosen from the coastal region to be processed using the ExtR retracking method. As a result of the retracking, biases of the magnitude of 2.3 and 7.7 bins (respectively equivalent to 1.0774 and 3.6069 m in SSH) were found between the ExtR-derived range measurements and those of original gates (Fig. 4, bottom).

In Table 4, the results of the post-processing algorithm (including instrumental and atmospheric corrections, as well as the application of ExtR) are summarized. These results are calculated from the mean residual values, which are computed by subtracting the tide gauge measurements from the final SSH values derived after applying the post-processing algorithm to the multimission observations of (i) 360 cycles of T/P, (ii) 260 cycles of Jason-1, (iii) 120 cycles of Jason-2, (iv) 10 cycles of ERS-1 and (v) 160 cycles of GFO over our study areas. Table 4 reports minimum, maximum and mean SSH residuals derived from each satellite before and after applying the post-processing corrections. Error values were computed from the differences between altimeter-derived SSHs and tide gauge measurements (magnitude of residuals). Considering the results of Table 4, it can be seen that the post-processing algorithm significantly improves SSH estimations over these regions.

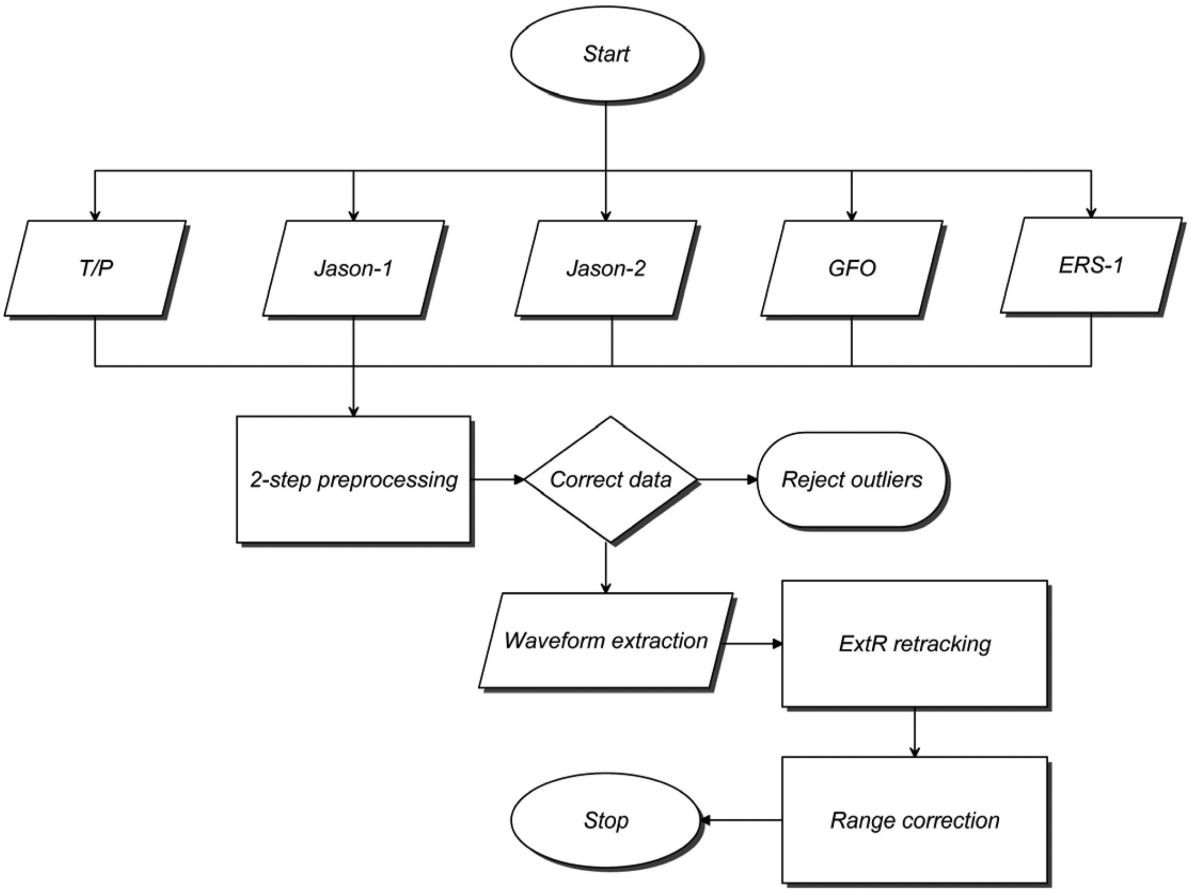

Figure 3. Flowchart of the ExtR retracking process (for details of the algorithm, we refer to Khaki *et al.* 2014).

Table 3. Sample statistics of the altimetry-derived range differences over the Persian Gulf and the Caspian Sea before and after the application of the ExtR technique (units in metre).

Area	Altimetry grid data	Maximum	Mean	RMSE	STD	Range improvement (per cent)
Persian Gulf	Before retracking	0.5660	0.3256	0.5701	0.0362	–
	After retracking	0.2849	0.1320	0.3714	0.0315	12.98
Caspian Sea	Before retracking	0.7158	0.4096	0.6933	0.0414	–
	After retracking	0.3734	0.2248	0.4686	0.0291	29.71

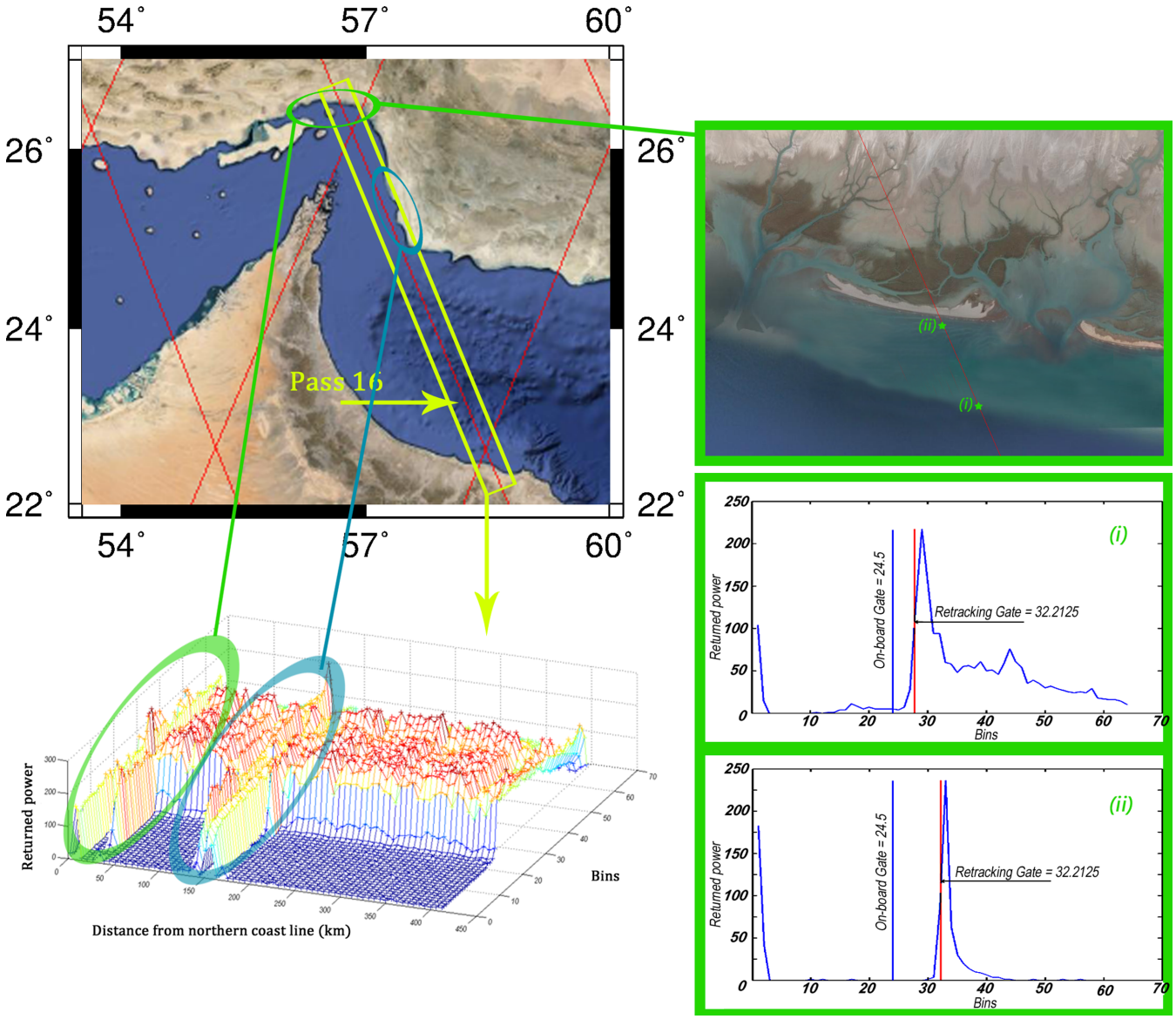

Figure 4. Sample waveforms belonging to pass 16 of cycle 26, observed by Jason-2 over the Persian Gulf; (top-left) represents the location of the pass, where the two green and blue ellipses indicate two selected coastal areas. (Bottom-left) indicates the observed waveforms by Jason-2, where those of coastal areas on the top are shown by the same coloured ellipses. (Top-right) indicates the position of two waveforms [(i) and (ii)] that are sampled over the shallow depth coastal area. (Bottom-right) represents the two waveforms in the top-right graph, where the ExtR estimated gates are compared to the original tracking gates.

4 GRAVITY ANOMALY

After applying the ExtR retracking procedure to all available altimetry-derived waveforms, the improved SSH estimates were converted to gravity anomaly maps. The implemented algorithm here is based on the remove–restore techniques used by many other methods for gravity field recovery from altimetry observation (e.g. Sandwell & Smith 1997, 2009; Hwang *et al.* 1998). Here a reference geoid model, the global geopotential model of EGM2008 up to spherical harmonic degree and order 2160, was removed from sea surface height profiles (Nerem 1994). This was done since extracting the shorter wavelength (∼5–10 km) of the gravity field, where satellite altimetry measurements are more sensitive, was of interest. The removed geoid values (using EGM2008) were restored later to derive full spectrum gravity anomalies. Therafter, derivatives of the ascending and descending part of each along-track altimetry profile were computed. Consequently, two grids of slope profiles

Table 4. A summary of statistics derived from comparisons between SSH values before and after applying corrections (units are in millimetre).

		Persian Gulf				Caspian Sea			
	Satellite	Min	Max	Mean	Error (per cent)	Min	Max	Mean	Error (per cent)
Before	T/P	23.48	61.39	30.89	9.71	22.94	56.60	33.62	13.89
	Jason-1	21.37	56.34	28.17	9.06	19.98	49.92	28.39	11.73
	Jason-2	18.10	55.06	23.84	7.23	17.63	40.65	24.40	10.30
	GFO	18.95	58.42	27.93	7.70	18.01	63.65	26.95	10.85
	ERS-1	21.67	61.48	31.64	10.34	22.15	57.21	35.43	15.43
After	T/P	7.23	32.79	14.66	5.25	9.41	38.11	17.93	5.02
	Jason-1	6.97	37.55	13.90	4.88	8.71	52.34	15.04	6.43
	Jason-2	3.81	24.41	10.01	3.24	4.18	28.19	12.61	3.23
	GFO	5.30	30.57	12.31	3.17	5.04	33.48	14.46	4.59
	ERS-1	9.17	43.63	18.43	5.79	11.36	59.02	21.85	7.56

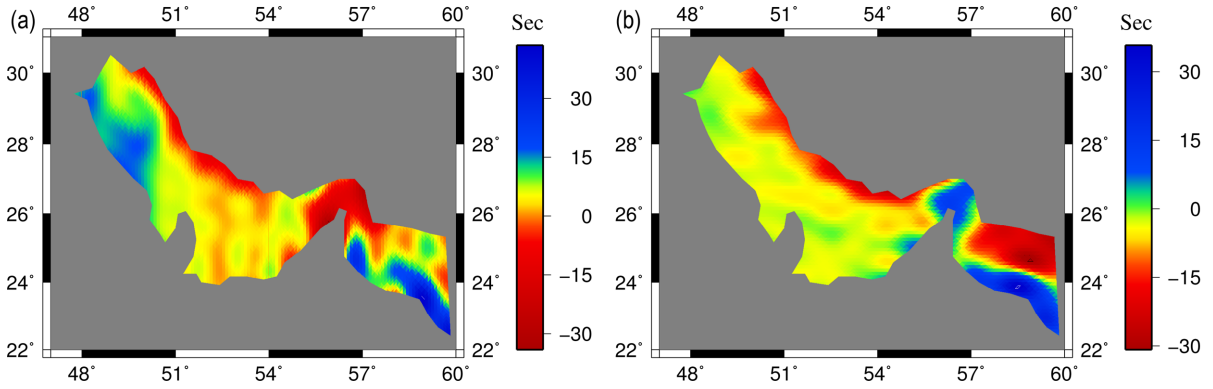

Figure 5. Deflections of the vertical over the Persian Gulf where (a) represents the east–west components and (b) represents the north–south components of deflections of the vertical. The maps are computed following the approach in Sandwell & Smith (1997), while considering the ExtR post-processed altimetry observations as its inputs.

(data along-track), including the ascending and descending parts were formed. Sandwell & Smith (1997) noted that using along-track derivatives from the altimeter profiles suppresses the long-wavelength radial orbit-errors, and this advantage was considered in our computations (see also Nerem 1994).

Gridding of the gravity anomaly data was motivated by two major facts, (i) to cover the study area completely, since the satellite tracks only cover the footprint locations (see Fig. 2) and (ii) to extract gravity anomalies from the observations of five satellite altimetry missions (including T/P, Jason-1, Jason-2, GFO and ERS-1) with different footprints, which necessitates the collocation of measurements. Therefore, the computed along-track slope values were interpolated on a regular grid. In this study, we used the moving surface spline interpolation technique (as in, Deng & Tang 2011), which combines a biharmonic spline interpolation algorithm with an application of the Green's function (e.g. Sandwell 1987). The technique is widely accepted for its high precision, simplicity and flexibility since it considerably reduces the number of extraneous inflection points (Wessel & Bercovici 1998), and also reduces the computational time (by choosing the nearest data points to the interpolation-grid position at each time, Deng & Tang 2011). Considering the applied methodology for gravity computation from gridded altimetric-derived surface slope data, which uses iterative least-squares adjustment, more satellite observations, and subsequently, more accurate gravity anomaly grids can be obtained.

For both study areas, grids with 0.05 degree grid-step were formed, which approximately correspond to 5.5 km spatial resolution. Hence, in each particular location, a total of 10 gridded sea surface slope values (two types of ascending and descending grid values corresponding to the five satellite missions) were derived by interpolating between the slope profiles. It should be mentioned here that various smoothing and noise elimination techniques have already been applied to the SSH estimations before computing the surface slopes. Two of these were applied before the retracking process: outliers detection and elimination of unwanted waveforms. The mentioned two-step preprocessing, especially helped us to smooth along-track SSH profiles. Afterwards, to deal with those SSH estimations that are not in the range of other track lines, a linear trend was fitted to the time-series. Then those points that fell out of the five to eight times of the standard deviations were eliminated. This method of noise reduction was applied in an iterative manner until the estimated RMSE were less than an arbitrary threshold value. After implementing both smoothing algorithms and noise eliminating processes, an iterative process was then applied to estimate deflections of the vertical at each grid location (see, Sandwell & Smith 2009, for more details). This procedure was repeated for both study areas of the Persian Gulf and the Caspian Sea, where the ExtR-derived sea surface slopes were converted into two grids of deflections of the vertical, representing the north–south (ξ) and east–west component (η) of deflections of the vertical.

5 RESULTS

5.1 Gravity anomaly within the Persian Gulf

In this section, first the altimeter-derived gravity anomalies are compared to ship-borne free air gravity anomaly profiles. This is then

followed by discussing the results of deflections of the vertical and gravity anomaly estimates. Over the Persian Gulf, the high-density waveform observations of the T/P, Jason-1 and Jason-2, GFO and ERS-1 altimetry missions were used (see Fig. 1). Table 1 summarizes the applied data sets with their cycles and passes numbers.

For completeness, in Fig. 5, deflections of the vertical are shown, where Fig. 5(a) represents the east–west components, and Fig. 5(b) represents the corresponding north–south components. The range of east–west and north–south profiles of the deflections of the vertical are found to be $-33.84''$ to $45.12''$ and $-31.06''$ to $34.54''$, respectively. Fig. 5 indicates more complex deflections of the vertical variability close to the coastlines, especially in the northern part of the Persian Gulf.

Satellite altimetry-derived gravity anomalies over the Persian Gulf were estimated following Sandwell & Smith (2009), with the ExtR-derived altimetry observations used as input (see Fig. 6a). The results indicate a significant improvement in estimation of gravity anomalies with a mean improvement of 7.5 mGal over the coastal area of the Persian Gulf after application of ExtR. Gravity anomaly residuals, derived as the difference between ship-borne gravity anomalies and original altimetry-derived gravity anomalies as well as gravity anomalies after application of ExtR, are shown in Figs 6(b) and (c), respectively. It is evident that using ExtR decreased the errors especially over northern coastlines, where the amplitude of noise is higher than the other parts. Furthermore, one can find significant differences in Figs 6(b) and (c) especially over the south–west and east parts of the Persian Gulf. These differences are the result of the ExtR retracking algorithm, whose influence was found significant over these complex geographic regions. This complexity includes: land contamination in the footprint of altimeters and the shallow water depth (∼20 m for this case), for example, over south–west of the Persian Gulf, as well as considerable tidal effect (and strong currents) in the east part of the Oman Gulf (where the Gulf meets the Indian Ocean). Fig. 6 also indicates that the differences of gravity anomaly after application of ExtR was of an acceptable range.

A visual comparison of the altimetry-derived and ship-borne free air gravity anomalies is presented in Fig. 7. Sample profiles in Fig. 7 were chosen out of the total of 61 profiles, whose tracks are shown in Fig. 2. Graphs on top of Figs 7(a)–(i) represent sample profiles of the computed gravity anomalies in blue and ship-borne measurements in red. The locations of sampled profiles are illustrated with the white tracks in Fig. 2. The bottom graphs of Figs 7(a)–(i) represent residuals of the altimetry-derived and ship-borne profiles (blue and red curves on top). It can be seen that the altimeter-derived gravity anomalies match fairly well the free-air gravity anomalies derived from ship-borne measurements. In Table 5, the numerical values of maximum, mean, rms and relative improvement of the residuals in Fig. 7 before and after implementing the ExtR processing algorithm are summarized. These values were computed by subtracting altimetry-derived gravity from the ship-borne data.

Considering the statistics in Table 5, it can be seen that the rms differences between altimetry- and ship-borne-gravity anomalies improved (by up to 96 per cent) after application of the ExtR post-processing. A maximum rms of 4.4069 mGal for the track g (see Table 5) was obtained, a magnitude acceptable for many gravity applications (e.g. Sandwell & Smith 1997). The magnitude of this rms difference before implementing ExtR was 11.3505 mGal. The improvements listed in this table represent relative reductions of the rms differences. Besides, the selected profiles residuals for 61 profiles (where ship-borne data were available) were calculated, resulting into a maximum difference of 14.9347 mGal and a

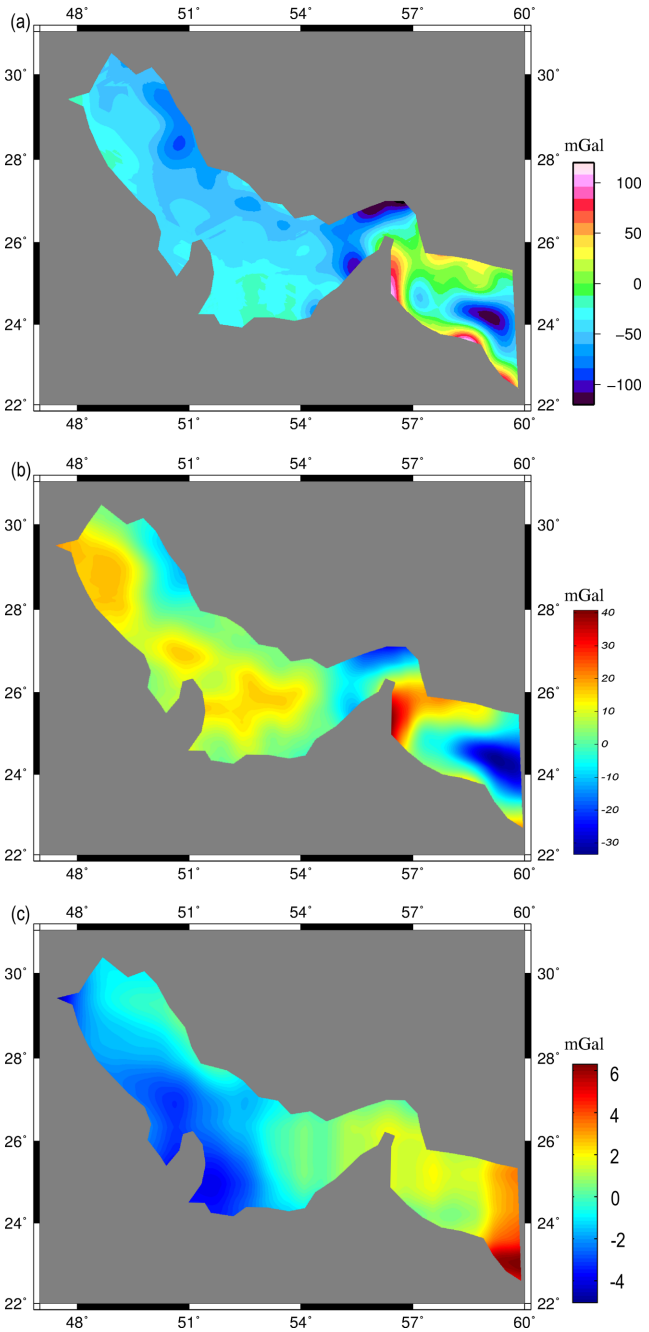

Figure 6. (a) Represents the marine (altimetry derived) gravity anomaly over the Persian Gulf using the ExtR-derived SSH observations. The differences between ship-borne gravity anomalies and altimetry-derived gravity anomalies are shown in (b) and (c), where for (b) marine altimetry gravity are derived from original data and in (c) after application of ExtR.

corresponding mean value of 0.7615 mGal. Since the acceptable accuracy of the altimetry-derived gravity estimations was achieved, estimations of deflections of the vertical and gravity anomalies covering the whole area of the Caspian Sea are discussed next.

5.2 Gravity anomaly within the Caspian Sea

Altimetry-derived gravity computations for the Caspian Sea are repeated using different passes of the five satellite altimetry missions.

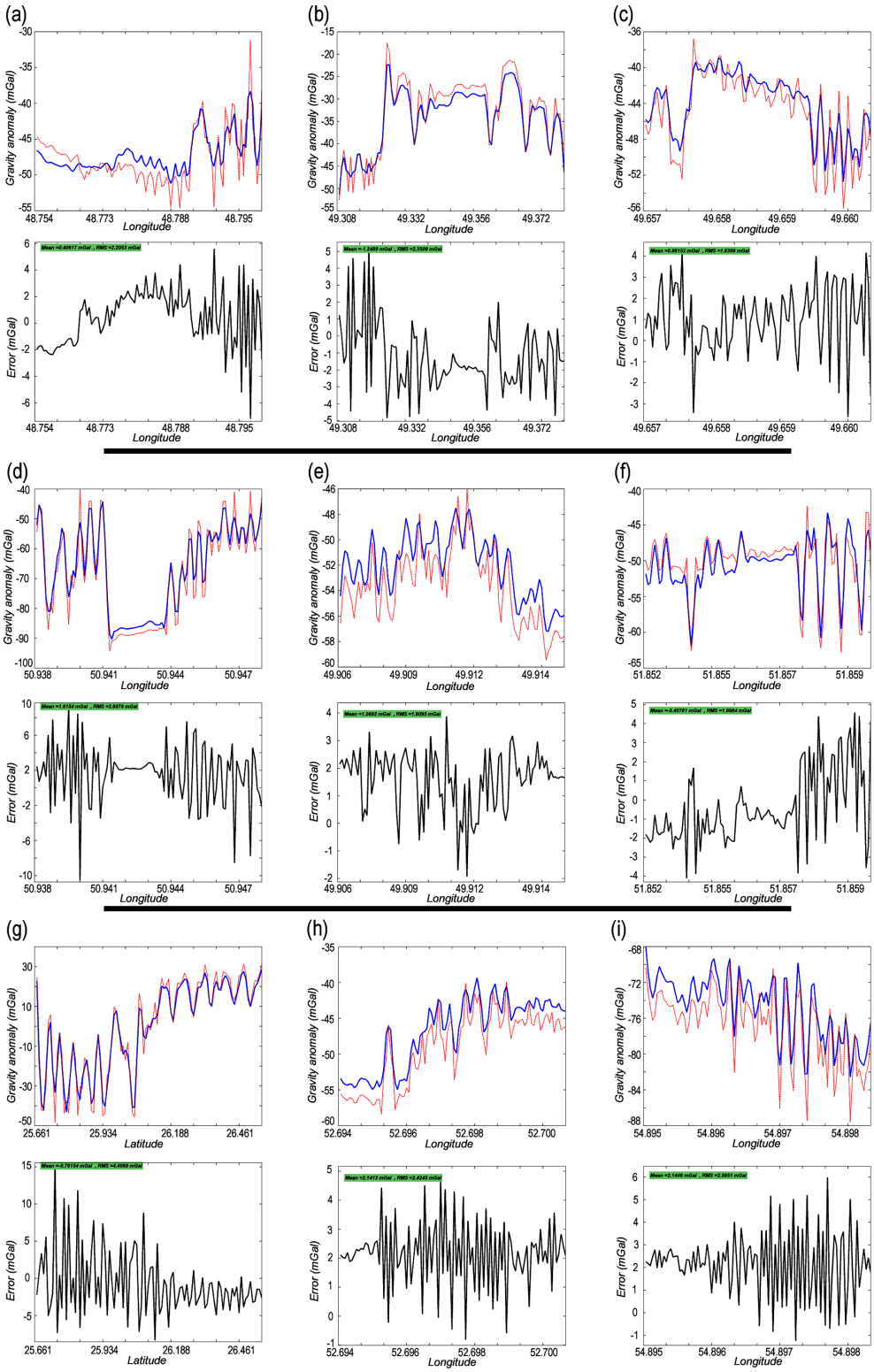

Figure 7. Comparison between ship-borne gravity anomaly (red) and satellite-derived gravity anomaly (blue) over the Persian Gulf along the selected ship-tracks indicated in Fig. 2. For each figure (a)–(h), the top graph represents the comparison between altimetry-derived and ship-borne gravity anomalies, and the bottom graphs show their residuals including the mean and rms values. Please note that all the numbers in green boxes also are represented in Table 5.

Table 2 contains details about the number of cycles and passes used in this study.

To validate the altimetry-derived results over the Caspian Sea, they were compared with the global geopotential model EGM2008. This comparison provided an assessment of the possible bias of the altimetry-derived gravity anomalies. To emphasize the importance of the application of the ExtR processing, both altimeter-derived gravity anomalies before and after application of ExtR were also

Table 5. A summary of the statistics derived from Fig. 5. The table represents the maximum, mean value and rms of the residual derived by subtracting the altimetry-derived gravity anomalies from those of ship-borne free air observations over the Persian Gulf.

	Without using ExtR			Using ExtR			
Index profile*	Max (mGal)	Mean (mGal)	rms (mGal)	Max (mGal)	Mean (mGal)	rms (mGal)	Improvements (per cent)
a	9.0427	6.1022	9.0305	5.7038	0.4062	2.2053	94.03
b	7.9123	2.3805	5.0892	5.1320	1.2489	2.3509	78.66
c	7.1598	6.3861	9.6285	4.1901	0.9815	1.8399	96.34
d	12.7188	8.7918	10.1473	9.2515	1.6154	3.8079	85.91
e	8.2275	3.8582	6.0720	3.9601	1.5692	1.9095	90.11
f	7.0230	4.8745	7.2167	4.4026	0.4078	1.9984	92.33
g	17.5492	5.9816	11.3505	14.9347	0.7615	4.4069	84.92
h	11.3001	7.3775	8.9828	4.6604	2.1413	2.4245	92.71
i	8.9326	6.9604	9.2164	5.0771	1.5955	2.2648	93.96

*Please note that the indices (a)–(i) in this table refer to the subfigures in Fig. 7.

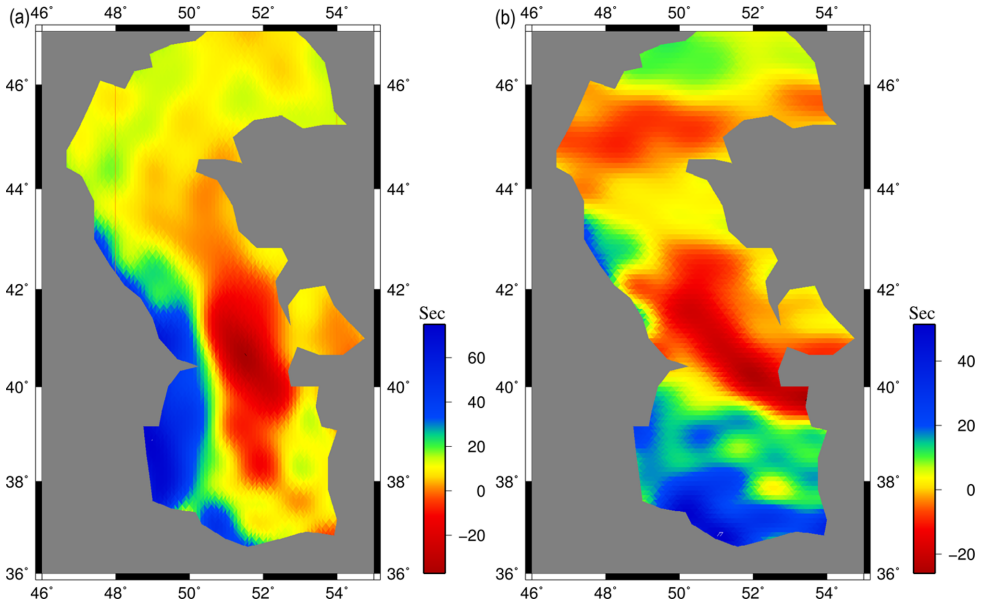

Figure 8. Deflections of the vertical over the Caspian Sea where (a) represents the east–west components, and (b) represents the north–south components of deflections of the vertical.

compared. Similar to Fig. 6, Fig. 8 includes deflections of the vertical, but over the Caspian Sea, where the east–west components are shown in Fig. 8(a), and the north–south components in Fig. 8(b). Both results show a short wavelength signal in deflections of the vertical mainly concentrated over the southern part of the Caspian Sea, which likely reflect the short wavelength variation in geoid due to the marginal shape of the two plates meeting around this region (see e.g. Jackson *et al.* 2002).

The altimetry-derived gravity anomaly without and with application of the ExtR retracking are shown respectively in Figs 9(a) and (b). Fig. 9 also contains the differences between original altimetry gravity anomalies and global geopotential model EGM2008 (Fig. 9c), as well as the difference between altimetry-derived gravity anomalies using ExtR algorithm and global geopotential model EGM2008 (Fig. 9d). Comparing Fig. 9(a) with Fig. 9(b), it can be seen that after the application of the ExtR post-processing, smoother gravity fields are derived over the entire Caspian Sea, particularly over the northern part that is predominately frozen during the cold seasons. As an example, between latitude 45°N–47°N, the ExtR-derived SSH improved altimetry-derived gravity anomaly estimations approximately by 8 mGal. On the other hand, over the central part of the Caspian Sea, where the situation is more stable with deeper water, maximum impact of ExtR was found to be 2.8450 mGal. The gravity anomaly differences in Figs 9(c) and (d) serve as a numerical control on the correctness of the performed computations, and the residuals cannot be interpreted as the validation performed in Figs 7(b) and (c).

In Table 6, the statistics (minimum, maximum, mean and standard deviation) of the gravity estimation differences before and after application of the ExtR technique are reported. The values were computed from differences between the altimetry-derived gravity anomaly and global geopotential model EGM2008. The results of Table 6 indicate an improvement in the differences of extracted gravity anomalies after application of ExtR. From the numerical results, particularly along the coastlines with complex topography as well as shallow waters, it seems that an application of retracking before estimating gravity anomalies is highly beneficial.

6 SUMMARY AND CONCLUSION

Due to the vast coverage, fairly high accuracy and its ease of access, satellite radar altimetry observations may be used for many geophysical applications especially to estimate gravity fields over water bodies. In this study, a variety of altimetry observations from the T/P, Jason-1, Jason-2, GFO and ERS-1 missions over the Persian Gulf

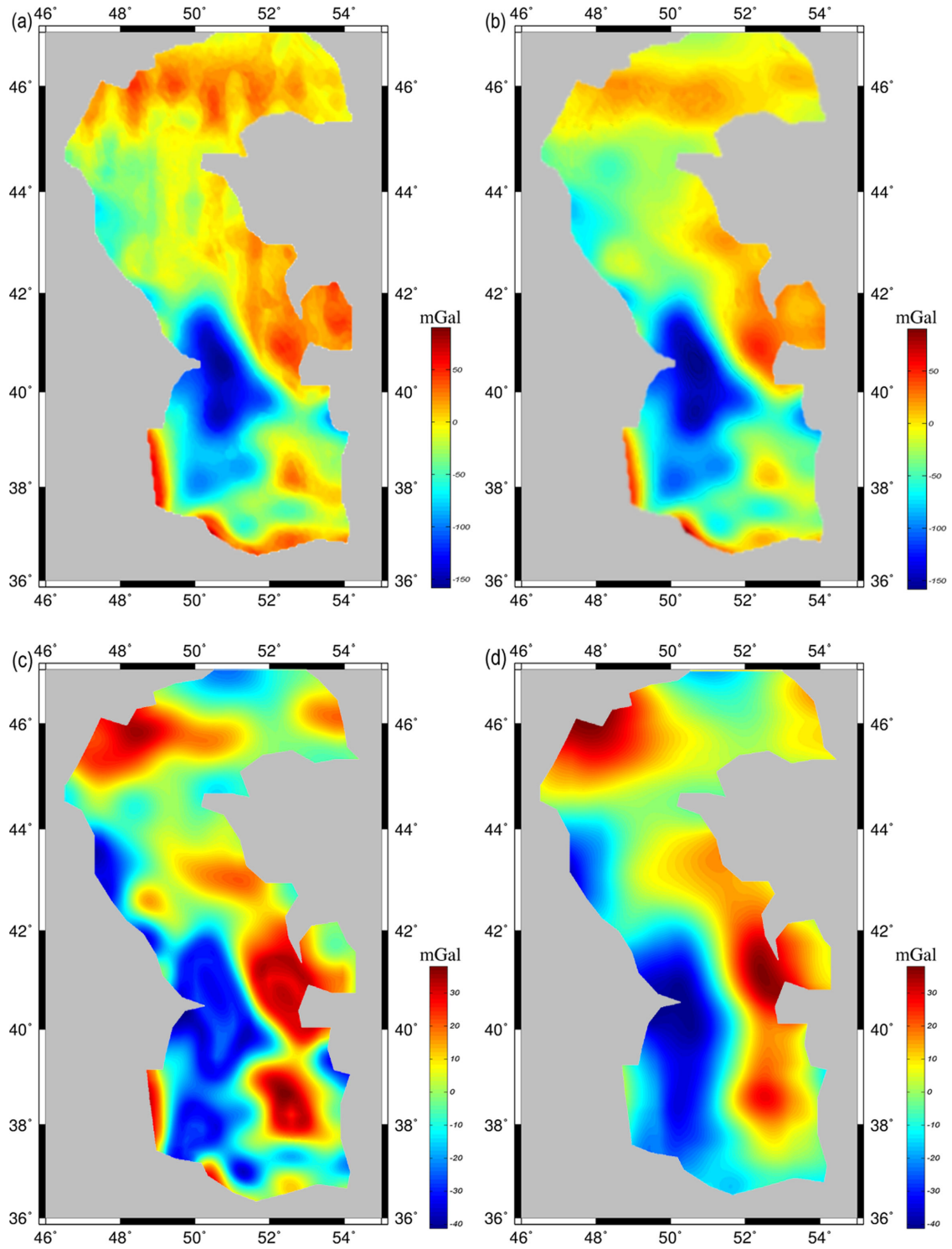

Figure 9. Marine gravity anomaly over the Caspian Sea before (a) and after (b) implementing the ExtR process. The difference between original altimetry-derived gravity anomalies and global geopotential model is shown in (c); the difference between altimetry-derived gravity anomalies using ExtR algorithm and global geopotential model is shown in (d). The graphs in (c) and (d) serve as numerical check for the estimated altimetry-derived gravity anomalies of (a) and (b).

and the Caspian Sea were used to extract gravity anomalies. Such estimation was realized by applying a remove–compute–restore algorithm based on the FFT conversion (Sandwell & Smith 2009) to estimate deflections of the vertical and subsequently to derive gravity anomalies. Using the altimeter data, first the geoid slope then east–west and north–south components of the deflections of the vertical were computed following Sandwell & Smith (1997).

Considering the unique properties of the study areas, that is, overall shallow depth of the Persian Gulf and an often frozen region over the northern part of the Caspian Sea, altimetry-derived SSH

Table 6. Descriptive statistics of the altimeter-derived gravity anomaly before and after application of the ExtR retracking over Caspian Sea (units in mGal).

Altimetry grid data	Minimum	Maximum	Mean	STD
Before retracking	−143.4863	67.6124	9.2842	26.1091
After retracking	−152.0776	61.5562	6.0758	25.3785

measurements, based on the default waveform-gate assumption and the on-board retracking algorithm, display limited precision. Therefore, a recently developed waveform retracking technique (ExtR, Khaki *et al.* 2014) was applied to improve the accuracy of range estimates, and subsequently SSH estimates. The errors computed after applying our post-processing algorithm (while applying all range corrections) over the study areas varied for each satellite, and we found the highest value belongs to the ERS-1 data set over the Caspian Sea (15.43 per cent). The results showed that total improvement caused by applying the ExtR retracking algorithm over the Persian Gulf and the Caspian Sea respectively are 12.98 and 29.71 per cent. Also the numerical results indicated that using ExtR post-processing significantly impacts on the estimation of gravity anomalies. This improvement over the Persian Gulf was found to reach up to 84.92 per cent with a maximum of absolute rms of 4.4069 mGal, and over the northern part of the Caspian Sea, this value was found to be 8.5186 mGal. In summary, the proposed algorithm in this paper, improved the accuracy of altimetry-derived gravity anomaly computation up to 89 per cent in our case studies and this is mostly because of the post-processing algorithm applied on satellite radar altimetry observations. During the estimation of gravity anomalies using altimetry observation over both the Persian Gulf and the Caspian Sea, retracking provided considerable improvements but there are still considerable differences that require the use of additional data sources. We therefore suggest using additional data sources in future studies for dealing with the mentioned differences. These further data may include land and marine gravimetry data within the coastal area, or geoid height measurements derived by GPS stations.

ACKNOWLEDGEMENTS

The authors would like to thank Prof J. Trampert (EiC), Prof B. Vermeersen (Editor) and two anonymous reviewers for their helpful comments, which improved the quality of this paper. We also would like to express our genuine thanks to Prof D.T. Sandwell (University of California, San Diego) and Prof W.H.F. Smith (NOAA; National Oceanic and Atmospheric Administration) for their kind guidance, warm encouragements and helpful comments. E. Forootan is grateful for the research grant from the German Aerospace Center (DLR, D-SAT project - Fkz.: 50 LZ 1402) and the research grant provided by TIGeR/WASM, Curtin University (Australia). We are grateful to the TOPEX/Poseidon, Jason-1, Jason-2, GFO and ERS-1 data sets downloaded from http://podaac.jpl.nasa.gov, http://avisoftp.cnes.fr and http://www.star.nesdis.noaa.gov. This work is a TIGeR publication No. 624.

REFERENCES

Andersen, O. & Kundsen, P., 2000. The role of satellite altimetry in gravity field modeling in coastal areas, *Phys. Chem. Earth (A),* **25**(1), 17–24.

Andersen, O., Berry, P., Freeman, J., Lemoine, F.G., Lutsckhe, S., Jakobsen, F. & Butts, M., 2008. Satellite altimetry and GRACE gravimetry for studies of annual water storage variations in Bangladesh, *Terr. Atmos. Ocean. Sci.,* **19**(1–2), 47–52.

Andersen, O.B., Knudsen, P. & Berry, P., 2010. The DNSC08GRA global marine gravity field from double retracked satellite altimetry, *J. Geod.,* **84**(3), doi:10.1007/s00190-009-0355-9.

Benada, J.R., 1997. *PODAAC Merged GDR (TOPEX/POSEIDON) Generation B Users Handbook*, Version 2.0. JPL D-11007. Jet Propulsion Laboratory, California Institute of Technology.

Berry, P.A.M., Garlick, J.D., Freeman, J.A. & Mathers, E.L., 2005. Global inland water monitoring from multi-mission altimetery, *Geophys. Res. Lett.,* **32,** L16401, doi:10.1029/2005GL022814.

Birkett, C.M., Mertes, L.A.K., Dunne, T., Costa, M.H. & Jasinski, M.J., 2002. Surface water dynamics in the Amazon Basin: application of satellite radar altimetry, *J. geophys. Res.*, **107**, doi:10.1029/2001JD000609.

Brown, G.S., 1977. The average impulse response of a rough surface and its applications, *IEEE Trans. Antennas Propag.,* **25,** 67–74.

Cande, S.C., Stock, J.M., Mueller, R.D. & Ishihara, T., 2000. Cenozoic motion between East and West Antarctica, *Nature,* **404,** 145–150.

Cazenave, A. & Royer, J.Y., 2001. Applications to marine geophysics, in *Satellite Altimetry and Earth Sciences: A Handbook of Techniques and Applications*, pp. 407–440, eds Fu, L.L. & Cazenave, A., Academic Press.

Davis, C.H., 1995. Growth of the Greenland ice sheet: a performance assessment of altimeter retracking algorithms, *IEEE Trans. Geosci. Remote Sens.,* **33**(5), 1108–1116.

Davis, C.H., 1997. A robust threshold retracking algorithm for measuring ice-sheet surface elevation change from satellite radar altimeters, *IEEE Trans. Geosci. Remote Sens.,* **35**(4), doi:10.1109/36.602540.

Deng, X. & Tang, Z.A., 2011. Moving surface spline interpolation based on Greens function, *Math. Geosci.,* **43,** 663–680.

Fairhead, J.D., Green, C.M. & Odegard, M.E., 2001. Satellite-derived gravity having an impact on marine exploration, *Leading Edge,* **20,** 873–876.

Fernandes, M.J., Lázaro, C., Nunes, A.L. & Scharroo, R., 2014. Atmospheric corrections for altimetry studies over inland water, *Remote Sens.,* **6**(6), 4952–4997.

Forootan, E., Rietbroek, R., Kusche, J., Sharifi, M.A., Awange, J., Schmidt, M., Omondi, P. & Famiglietti, J., 2014. Separation of large scale water storage patterns over Iran using GRACE, altimetry and hydrological data, *Remote Sens. Environ.,* **140,** 580–595.

Fu, L.L., Christensen, E. & Yamarone, C.A., 1994. TOPEX/POSEIDON mission overview, *J. geophys. Res.,* **99,** doi:10.1029/94JC01761.

Garcia, E.S., Sandwell, D.T. & Smith, W.H.F., 2014. Retracking CryoSat-2, Envisat and Jason-1 radar altimetry waveforms for improved gravity field recovery, *Geophys. J. Int.* **196**(3), 1402–1422.

Gille, S.T., 1994. Mean sea surface height of the Antarctic circumpolar current from Geosat data: method and application, *J. geophys. Res.,* **99,** 18 255–18 273.

Gomez-Enri, J., Vignudelli, S., Quartly, G., Gommenginger, C. & Benveniste, J., 2009. *Bringing satellite radar altimetry closer to shore. Remote Sensing, SPIE Newsroom*, doi:10.1117/2.1200908.1797.

Haxby, W.F., Kamer, G.D., LaBrecque, J.L. & Weissel, J.K., 1983. Digital images of combined oceanic and continental data sets and their use in tectonic studies, *EOS, Trans. Am. geophys. Un.,* **64,** 995–1004.

Hwang, C. & Hsu, H.Y., 2003. Marine gravity anomaly from satellite altimetry: a comparison of methods over shallow waters, in *Proceedings of International Workshop on Satellite Altimetry for Geodesy, Geophysics and Oceanography*, IAG symposium, Vol. 126, pp. 59–66.

Hwang, C. & Hsu, H.Y., 2008. Shallow-water gravity anomalies from satellite altimetry: case studies in the east China and Taiwan straiy, *J. Chin. Inst. Eng.,* **31**(5), 841–851.

Hwang, C., Kao, E.C. & Parsons, B., 1998. Global derivation of marine gravity anomalies from Seasat, Geosat, ERS-1 and TOPEX/POSEIDON altimeter data, *Geophys. J. Int.,* **134,** 449–459.

Jackson, L., Priestley, K., Allen, M. & Berberian, M., 2002. Active tectonics of the South Caspian Basin, *Geophys. J. Int.,* **148,** 214–245.

Khaki, M., Forootan, E. & Sharifi, M.A., 2014. Satellite radar altimetry waveform retracking over the Caspian Sea, *Int. J. Remote Sens.,* **35**(17), 6329–6356.

Kingdon, R., Hwang, C., Hsiao, Y.S. & Santos, M., 2007. Gravity anomalies from retracked ERS and geosat altimetry over the Great Lakes: accuracy assessment and problems, *Terr. Atmos. Ocean. Sci.,* **19**(1–2), 93–101.

Kouraev, A.V. *et al.*, 2011. *Satellite Altimetry Applications in the Caspian Sea*, Springer, Chap. 13, pp. 331–366.

Lambeck, K., Esat, T.M. & Potter, E.K., 2002. Links between climate and sea levels for the past three million years. *Nature,* **419**(6903), 199–206.

Lawver, L.A., Gahagan, L.M. & Coffin, M.F., 1992. The development of paleoseaways around Antarctica, in *The Antarctic Paleoenvironment: A Perspective on Global Change, Geophys. Monogr. Ser.*, Vol. 56, pp. 7–30, eds Kennett, J.P. & Warnke, D.A., AGU.

Lee, H., Shum, C.K., Yi, Y., Braun, A. & Kuo, C.-Y., 2008. Laurentia crustal motion observed using TOPEX/POSEIDON radar altimetry over land, *J. Geodyn.,* **46,** 182–193.

Marchenko, A., Tartachynska, Z. & Zazulyak, P., 2003. *Regional gravity field from TOPEX/POSEIDON, ERS-1, ERS-2 altimetry and BGI gravimetry data in the Mediterranean and Black Sea area*, National University Lviv Polytechnic, S. Bandera St., 12, Lviv, Ukraine.

Martin, T.V., Zwally, H., Brenner, A.C. & Bindschadler, R.A., 1983. Analysis and retracking of continental ice sheet radar altimeter waveforms, *J. geophys. Res.,* **88**(C3), 1608–1616.

Mayer-Gürr, T., 2006. *Gravitationsfeldbestimmung aus der Analyse kurzer Bahnbgen am Beispiel der Satellitenmissionen CHAMP und GRACE, Dissertation*, University of Bonn.

Nerem, R.S., 1994. Gravity model development for the TOPEX/POSEIDON: joint gravity models 1 and 2, *J. geophys. Res.,* **99,** 24 421–24 447.

Noreus, J.P., Nyborg, M.R. & Hayling, K.L., 1997. The gravity anomaly field in the Gulf of Bothnia spatially characterized from satellite altimetry and in situ measurements, *J. appl. Geophys.,* **37,** 67–84.

Ozyavas, A., Khan, S.D. & Casey, J.F., 2010. A possible connection of Caspian Sea level fluctuations with meteorological factors and seismicity, *Earth planet. Sci. Lett.,* **299,** 150–158.

Perotti, C.R., Carruba, S., Rinaldi, M., Bertozzi, G., Feltre, L. & Rahimi, M., 2011. The Qatar–South Fars arch development (Arabian Platform, Persian Gulf): insights from seismic interpretation and analogue modelling, in *New Frontiers in Tectonic Research - At the Midst of Plate Convergence*, ed. Schattner, U., InTech.

Safari, A., Sharifi, M.A., Amin, H., Foroughi, I. & Tenzer, R., 2014. Determining the gravitational gradient tensor using satellite-altimetry observations over the Persian Gulf, *Marine Geod.,* **37**(4), 404–418.

Sandwell, D.T., 1987. Biharmonic spline interpolation of Geos-3 and Seasat altimeter data, *Geophys. Res. Lett.,* **14**(2), 139–142.

Sandwell, D.T. & Smith, W.H.F., 1997. Marine gravity anomaly from Geosat and ERS 1 satellite altimetry, *J. geophys. Res.,* **102**(B5), 10 039–10 054.

Sandwell, D.T. & Smith, W.H.F., 2009. Global marine gravity from retracked Geosat and ERS-1 altimetry: ridge segmentation versus spreading rate, *J. geophys. Res.,* **114,** B01411, doi:10.1029/2008JB006008.

Sandwell, D.T., Müller, R.D., Smith, W.H., Garcia, E. & Francis, R., 2014. New global marine gravity model from CryoSat-2 and Jason-1 reveals buried tectonic structure, *Science,* **346**(6205), 65–67.

Sharifi, M.A., Forootan, E., Nikkhoo, M., Awange, J.L. & Najafi-Alamdari, M., 2013. A point-wise least squares spectral analysis (LSSA) of the Caspian Sea level fluctuations, using TOPEX/Poseidon and Jason-1 observations, *Adv. Space Res.,* **51**(5), 858–873.

Shum, C.K., Ries, J.C. & Tapley, B.D., 1995. The accuracy and applications of satellite altimetry, *Geophys. J. Int.,* **121,** 321–336.

Troitskaya, Y.I., Rybushkina, G.V. & Soustova, I.A., 2012. Satellite altimetry of inland water bodies, *Water Resour.*, **39,** 184–199.

Uebbing, B., Kusche, J. & Forootan, E., 2015. Waveform retracking for improving level estimations from Topex/Poseidon, Jason-1 and -2 altimetry observations over African lakes, *IEEE Trans. Geosci. Remote Sens.,* **53**(4), 2211–2224.

Wessel, P. & Bercovici, D., 1998. Interpolation with splines in tension: a Greens function approach, *Math. Geol.,* **30**(1), 77–93.

Wingham, D.J., Rapley, C.G. & Griffiths, H., 1986. New techniques in satellite altimeter tracking systems, in ESA Proceedings of the 1986 International Geoscience and Remote Sensing International Journal of Remote Sensing 6355 Downloaded by [93.129.93.155] at 12:13 17 September 2014 Symposium (IGARSS 86) on Remote Sensing, *Todays Solutions for Tomorrows Information Needs,* **3,** 1339–1344.

Zhang, M.M., 2009. Satellite radar altimetry for inland hydrologic studies, *PhD thesis*, The Ohio State University.